High-pressure STM studies of oxidation catalysis

Bobaru, Ş.C.

Chapter 6

Oxidation of Pt (100)

In this chapter the structure, chemistry and catalytic activity of the (100) surface of platinum is discussed. From the structural point of view there is an important difference with the Pt(111) surface discussed in Chapter 5, since the Pt(100) surface exhibits a reconstruction. We show that the CO oxidation reaction on this surface has two regimes of bistability, rather than just one. The first corresponds to the transition between the metallic surface and a surface oxide, similar to the scenario on the palladium surfaces in Chapter 3 and on Pt(111). The second is the traditional bistability of the Langmuir-Hinshelwood reaction on the metal surface. The surface oxide is found to be stable only at extremely low CO pressures, where it leads to little advantage over the reaction rate on the metal surface. The Langmuir-Hinshelwood reaction turns out to have spectacularly high conversion rates.

6.1 The quasi-hexagonal reconstruction

Structure

A clean Pt(100) surface undergoes a structural transformation from a bulk like terminated Pt(100)-(1×1) structure to the so-called Pt(100) hex reconstructed phase [1]. This reconstruction is favoured because it minimizes the surface free energy in absence of adsorbates.

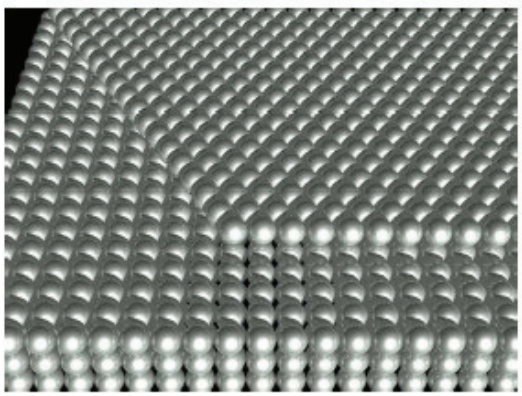

Figure 6.1: *The hex-reconstructed layer on top of the Pt(100)-(1x1) structure.*

The first reconstruction of a clean metal has been reported in 1965 for Pt(100) by Hagstrom et al. [2]. Since the LEED pattern showed the appearance of diffraction beams in (or near) multiples of the (1/5)-th order position, the authors called the new structure (1×5). In 1967, Fedak and

Gjostein observed a (1x5) reconstruction for Au(100) [3]. Soon after their observation these authors managed to resolve a splitting in the LEED spots for Au, indicating a (20×5) rather than (1×5) structure. Fedak and Gjostein have been the first to propose a hexagonal overlayer on the square substrate mesh as a model for the surface rearrangement [4]. A sharp (1×5) LEED pattern without splitting has been found for Ir(100) in 1969 by Grant [5]. In summary, the (100) faces of Au, Pt, and Ir have a surface reconstruction formed by a compact (quasi) hexagonal surface layer resting on top of the underlying square lattice. In each case the pattern exhibits a row-like structure, resulting from a regular structure in which every group of six top-layer atom rows covers the area of on five atom rows of the substrate.

In the case of Pt(100), two phases of reconstruction exists. Upon annealing to temperatures in the range of 400 K-1100 K, the unrotated phase designated as Pt (100)-hex is formed. Above 1100 K, a transformation occurs to a phase where the hexagonal layer is rotated 0.7º with respect to the underlying, square lattice, a structure referred to as Pt(100)-hex-R0.7º or, in matrix notation:

$$\begin{pmatrix} N & 1 \\ -1 & 5 \end{pmatrix}$$

where N is in the range of 12-14 [6].

The quasi-hex reconstruction of Pt(100) is lifted by adsorption of various gases (NO, CO, O2 and C_2H_4) resulting in adsorbate-covered (1x1) surface structures [7-16].

Origin

In order to explain the origin of the reconstruction one should take in consideration several interesting aspects of this platinum surface. First, this reconstruction is seen only at the end of 5d transition metal series, for the metals Ir, Pt, and Au, but not on their 4d counterparts (Rh, Pd, and Ag). Second, it has been shown that the (100) surfaces of the late 5d metals can be easily forced to switch between the reconstructed and unreconstructed phases by deposition and removal of small amounts of adsorbates, which indicates that the energy difference between the two phases is small. The (111) face of a face-centred crystal is usually the surface with the lowest free energy, so it may come as no surprise that the (100) surfaces prefer the reconstruction with a close-packed hexagonal overlayer. Of course, this argument completely ignores the unfavourable atomic stacking of a hexagonal layer on a lattice with square symmetry. In spite of the seeming

similarity between the hex-reconstructed Pt(100) surface and Pt(111), the work function on Pt(100) is lower than that on Pt (111) by as much as 0.5eV [17].
Ab initio calculations have suggested that the origin of quasi-hexagonal reconstruction lies in a relativistic effect. The calculations performed by Fiorentini et al. have shown that the reconstruction results from a delicate balance between surface-substrate mismatch and stress-related energy gain. Only in the case of 5d metals is the latter gain large enough to actually drive the reconstruction against the substrate resistance to misregistry, which is comparable for isoelectronic systems (e.g., Pd and Pt). The origin of the surface stress is the d-depletion at the surface accompanying the enhanced sp-hybridisation; the remarkable stress enhancement in 5d metals is due to the major relativistic effects in the 6s and 6p shells [18]. A similar effect drives the (110) surfaces of the same materials to the so-called missing-row reconstruction and stabilizes atomic chains of these materials in break-junction experiments [19].

6.2 Experimental

All the experiments described in this chapter have been performed using the Reactor-STM, which has been described in the introductory chapter. The surface has been prepared in UHV by cycles of 600 eV Ar^+ bombardment followed by annealing to ~800 K in 1×10^{-6} mbar O_2 and brief annealing in UHV around 1000 K. This procedure was repeated until a sharp LEED diffraction pattern was obtained, as illustrated in figure 6.2, reflecting the fivefold period of the Pt(100) hex-reconstructed surface. The cleanliness of the sample was checked with the STM. As shown in figure 6.3 atomically resolved, high-quality STM images have been obtained.

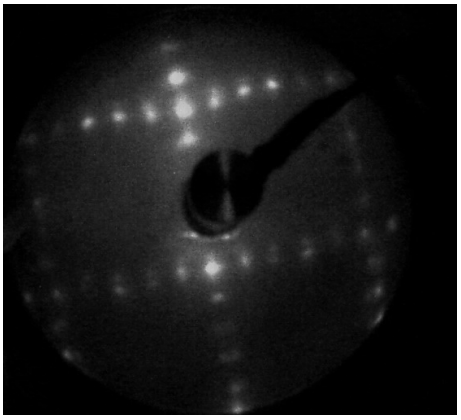

Figure 6.2: *Room temperature LEED pattern of the clean, hex-reconstructed Pt(100) surface. The electron beam energy was 60 eV.*

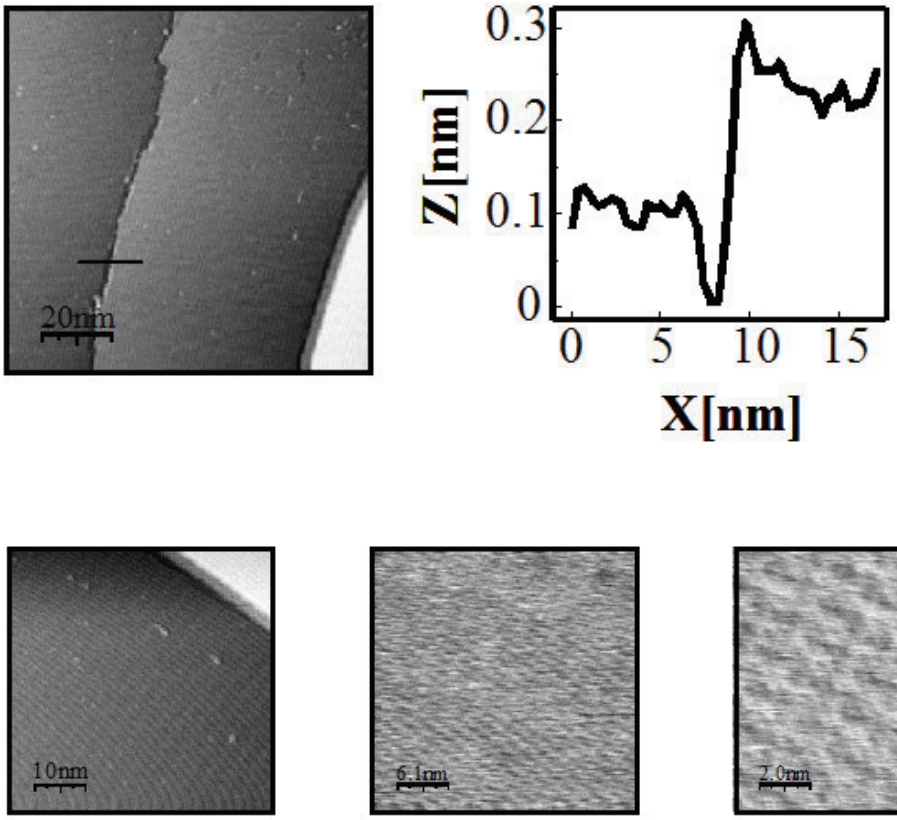

Figure 6.3: *Upper left: 100 nm × 100 nm STM image showing the clean Pt(100) surface in the poor vacuum of our Reactor-STM. The row-like features of the hexagonal reconstruction are clearly visible as stripes in the surface. Upper right: the cross-section along the line segment in the upper left image shows a step height of 2.0 Å, the expected value for Pt(100). Lower images: zooming in further, we have obtained STM images (50 nm× 50 nm, 30 nm × 30 nm, 10 nm × 10 nm) illustrating atomic-scale detail within the (5x20) unit cell of the hex-reconstructed Pt(100) surface.* V_t*=0.8 V,* I_t*= 0.2 nA*

6.3 Results and discussion

6.3.1 Interaction of CO with Pt(100)

As mentioned above, it is known that the hex-reconstruction is lifted by the adsorption of CO and several other adsorbates. Thiel et al. [20] have proposed the following mechanism for the removal of the reconstruction by CO adsorption at low temperature (400 K). This mechanism involves initial CO adsorption on the hex phase, which is followed by migration of CO, cluster formation, rapid hex→(1x1) conversion of the local substrate area, and trapping of the CO molecules on the resulting (1x1) patches. The

driving force for the CO-induced hex→(1x1) phase transition is the higher heat of adsorption of CO on the (1x1) phase compared to the reconstructed phase. Other STM studies have revealed that the transformation from the hex reconstruction to a CO-covered Pt(100)-(1x1) surface structure is indeed initiated by heterogeneous nucleation and that the growth of the (1x1) phase is highly anisotropic [15]. Figure 6.4 displays the (1x1) islands which have formed on the hex-reconstructed Pt(100) due to CO adsorption. The STM images have been acquired after the clean hex reconstructed surface was exposed to a 4:1 mixture of Ar and CO. The total pressure was 1.25 bar, and the temperature of the sample was 433 K. The height of the islands relative to the surrounding terrace was determined to be 2.0 Å, which is equal to the height of a monoatomic step as can be seen in the cross line profile from figure 6.4. From the STM images in figure 6.4 we see that the shape of the islands has a weak, square symmetry, showing that the hexagonal structure is indeed removed.

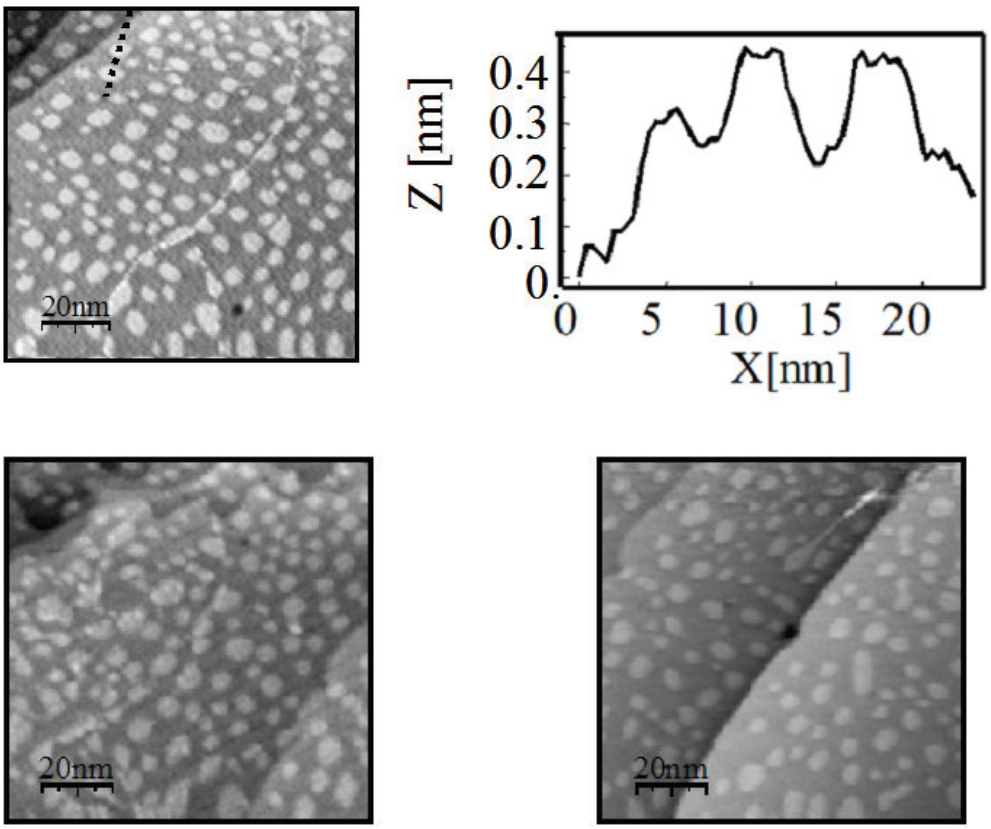

Figure 6.4: *STM images (100nm×100nm) illustrating the lifting of the hex-reconstruction due to CO adsorption at P_{CO} = 1.0 bar and at T = 433 K. The resulting (1x1) islands have a variety of sizes and different shapes with a weak, square symmetry. V_t=0.1 V, I_t= 0.2 nA*

Our measurements have shown that in a CO-rich flow the Pt(100) surface has a high mobility. The sizes and shapes of the adatom islands were observed to evolve in time, primarily via the coalescence dynamics resulting from spontaneous shape and position fluctuations of the islands. Once two islands had made contact with each other, they lowered their combined perimeter length and thereby their total free energy by fusing together into a single, compact island. In figure 6.5 we illustrate this process of rearrangements of the (1x1) adatom islands of the Pt (100) surface under a high CO partial pressure. If we compare image A with image G we see that many islands have changed their shape. The island sizes have remained almost unchanged, which indicates that Ostwald ripening is not strong under these conditions. In Figure 6.5 we also see that two coalescence events have occurred. The two adatom islands indicated in A by numbers 1 and 2 have coalesced, resulting in the formation of adatom island number 5 in image G. Similarly, islands 3 and 4 in image A have merged into adatom island number 6 in image G. In both cases two neighbouring islands fused together. The initial distances between their edges were 2.5 nm and 1.17 nm respectively. The island pairs have managed to bridge these distances and already evolve substantially towards a new, compact shape within the time interval between of approximately 10 minutes between images A and G. If we add the perimeters of islands 1 (12.7 nm) and 2 (26.6 nm) we obtain a sum of 39.3 nm that is substantially larger than the perimeter of the merged island 5 of 27.6 nm. A similar reduction in total perimeter length can be measured for the merger of islands 3 and 4. Images B-F show several intermediate stages in the encounter and coalescence of islands 3 and 4. In image B the two islands are still separated by 1.2 nm. Within a time interval of 3 minutes this distance has remained almost unchanged (C). After a further 2 minutes, the two islands have formed a connecting neck, resulting in the structure labelled 6 with a perimeter length of 34.0 nm, as seen in image D. This structure quickly reshaped itself. Within only 1 min the neck of the 6 structure has grown substantially in width as seen in image E, reducing the perimeter to a length of 31.3 nm. After an additional time of 2 min we arrived at image F in which structure 6 has an even more compact shape and a perimeter of 29.3 nm. The fact that the areas of the merged islands are not changing during their rearrangement to a more compact shape shows that also this part of the process does not involve exchange (evaporation and recondensation) of Pt atoms between the islands and their surroundings, but most probably this reshaping proceeds via edge diffusion of Pt atoms.

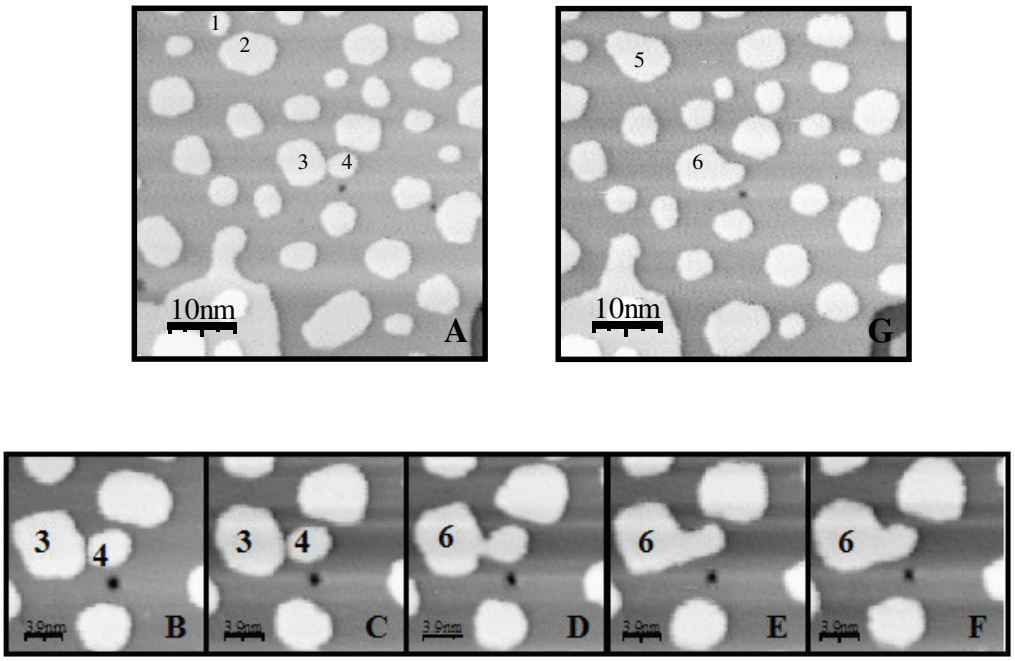

Figure 6.5: *STM images displaying the coalescence dynamics of adatom islands on an unreconstructed Pt(100) surface in CO-rich flow at atmospheric pressure (P_{CO} = 1.0 bar) and an elevated temperature of 368 K. V_t=0.1 V, I_t= 0.2 nA.*

Another example of the rapid dynamics of the unreconstructed Pt(100) surface is displayed in figure 6.6. In this case besides the coalescence process introduced above, we have also observed the opposite process: the break-up of a large structure into smaller-size features. Similar to the case introduced in figure 6.5 this process took place under CO-rich flow. Initially islands 2 and 3 coalesced with island 1 forming a complex structure with a very stretched and branched shape, as seen in image H2. This large structure decayed in time (images H3-H5) towards a more compact shape. Interestingly, the part formed by island 2 and most of island 1 was competing in this process with the part formed by island 3 and the lower left section of island 1. This competition actually led to a thinning and eventually even a rupture (image H6) of a narrow part that was originally within island 1. We might refer to this special type of event as 'coalescence-induced island break-up'. We stress that in this break-up process the total perimeter length was *not* increased. The stretched geometry made the total step length decrease when the island was separated into two more compact shapes.

In order to learn more about the smoothing process in a CO-rich flow we have calculated the step density in the images discussed above as well as images acquired at intermediate times (not shown). The result of this analysis is displayed in figure 6.7. The graph shows a clearly decreasing trend in the step density as a function of time.

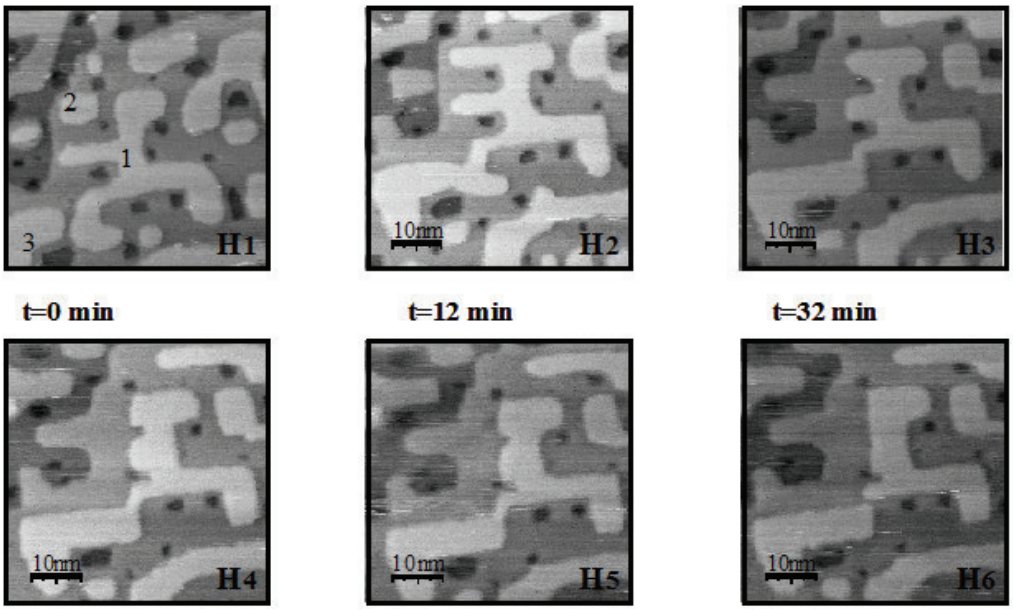

Figure 6.6: *STM images illustrating the evolution of a complex adatom island structure. As a consequence of the evolution towards a more compact shape, the central island breaks up into two smaller fragments. The size of the images is 50 nm × 50 nm.* V_t*=0.1 V,* I_t*= 0.2 nA.*

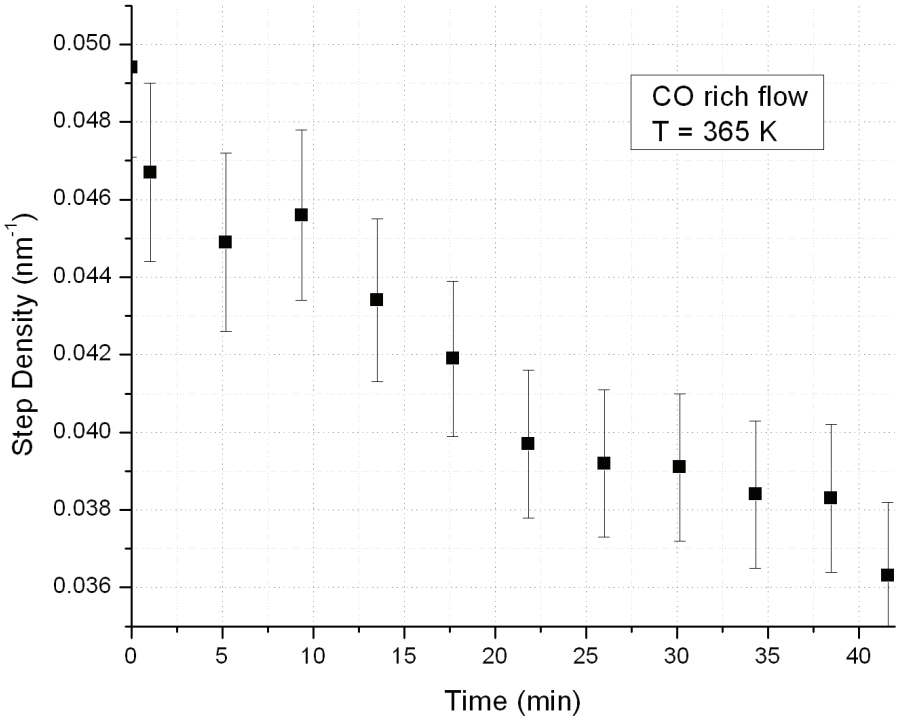

Figure 6.7: *The decrease of the step density in time in CO rich flow, measured from a series of STM images acquired in a flow of 1.25 bar of CO at a temperature of 365 K.*

Summarizing, based on the experimental evidence introduced in this section we conclude that exposure of the hex-reconstructed Pt(100) to atmospheric pressures of CO lifts the reconstruction. In this process, the excess Pt atoms expelled from the surface layer form adatom islands. Under the same conditions of high CO pressure and elevated temperature we observe that the adatom island pattern coarsens, mainly by coalescence dynamics, leading to a gradual smoothening of the surface.

6.3.2 Interaction of O_2 with Pt(100)

Since Pt(100) constitutes one of the low-Miller-index faces of platinum and the density of atoms on this surface is intermediate between those of the other two low-index surfaces, Pt(110) and Pt(111), we may expect that in an O_2-rich flow the (100) surface would show similar behaviour to these other surfaces (see ref. [21] for the (110) surface and Chapter 5 for the (111) surface). In particular, we expect the surface to oxidize at sufficiently high P_{O_2} and we expect this oxide surface to exhibit a higher reactivity towards CO oxidation.

Relatively little information is available in the literature about the interaction of O_2 with Pt (100), except for the fact that, similar to other gases, the oxygen lifts the hex- reconstruction. Early work by Griffiths and Norton [9,10] has revealed the existence of two surface phases depending on the atomic oxygen coverage. The first structure gives rise to a (3×1) LEED pattern and involves 0.51×10^{15} Pt atoms cm^{-2} that are displaced by 0.025 nm from bulk lattice positions. The other phase has a very complex LEED pattern, it shows a decrease in the work function compared with the (3×1) phase, and it involves 0.82×10^{15} Pt atoms cm^{-2} that are displaced by 0.025 nm. STM studies [15] describing the lifting of the reconstruction of Pt (100) –hex-R0.7° have suggested that the nucleation of the (1×1) islands may be initiated by the adsorption of oxygen molecules on the hex-R0.7° surface. The nucleation process is limited by the low sticking coefficient of oxygen on this surface, which is about four orders of magnitude lower than that for CO on the same surface. However, the oxygen sticking probability may be higher at step edges [22]. Figure 6.8 shows a STM images recorded on the CO-covered Pt(100) surface and its height profile histogram. From the histogram clearly can be seen that the step height from the adatom island down to the terrace is 2 Å corresponding to the step height of metallic platinum. When exposed to O_2 rich-flow the surface visibly roughness compared to the CO-covered surface as seen in STM images from figure 6.9. We have performed 30 additional cycles of exposure of the surface to a CO-rich gas flow and exposure to an O_2-rich flow and in each case find that the surface is significantly rougher in the O_2-rich flow than in the CO-rich flow.

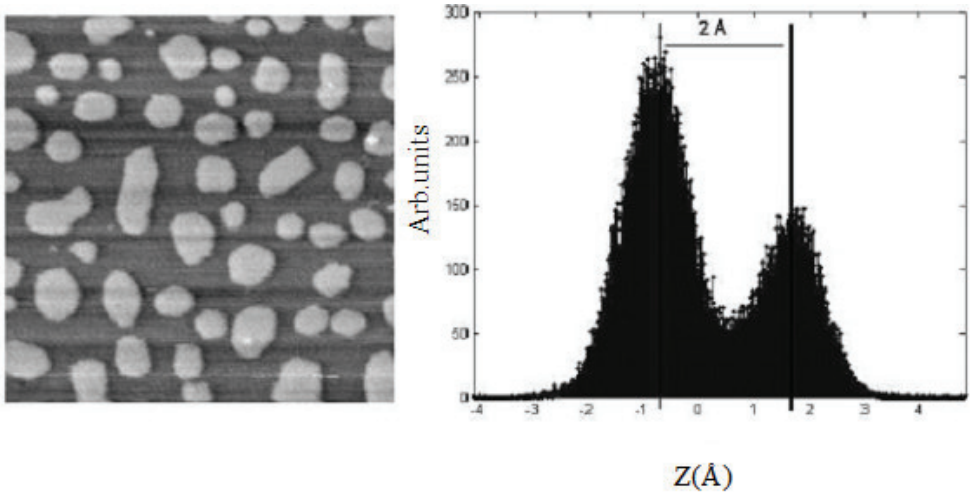

Figure 6.8: *STM image (50nm×50nm) and its histogram in CO rich-flow (1.12 bar) at T=418 K.*

As illustrated in figure 6.9 new structures are formed. In Fig. 6.9 we also show the height distribution for each image. The histograms show a variety of height differences, some of which may be close to multiples of the 0.20 nm step height of Pt(100) but others being completely different. We interpret the changes in the images and the new heights introduced upon exposure of the surface to high oxygen pressures as a strong indication that also this surface is oxidized, similar to Pt(110) and Pt(111).

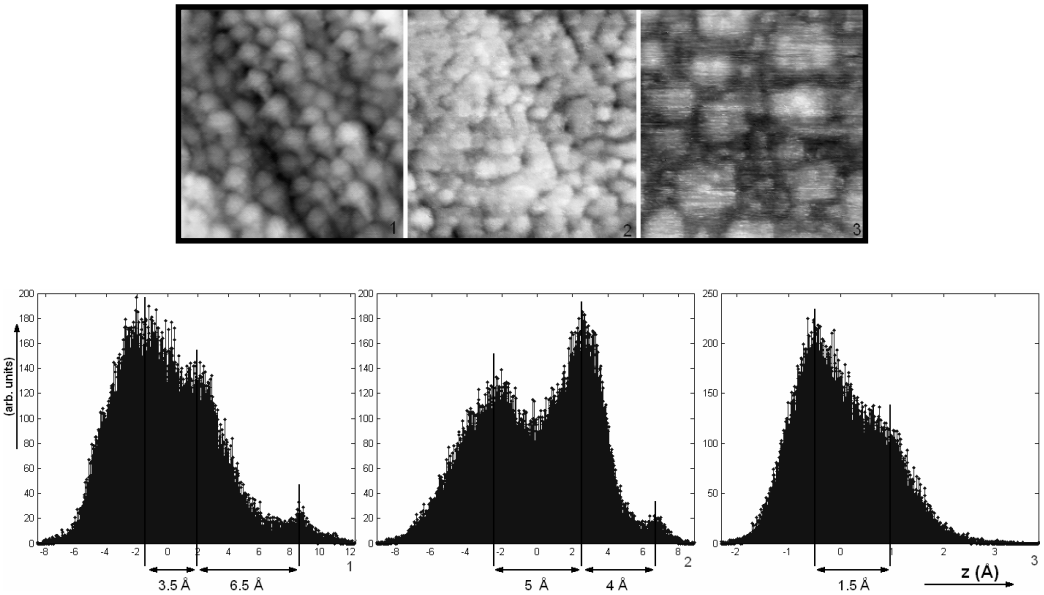

Figure 6.9: *Various oxygen-covered states of Pt (100) surface and the corresponding histograms .The size of the first 2 images is 100nm×100nm , while the size of image 3 is 30.5nm×30.5nm. The first 2 images have been acquired at 1.25 total pressure (1.16 bar of O_2). Image 3 has been recorded in a ratio O_2:CO equal to 6. The temperature was 403 K (image1), 408 K (image 2) and 368K (image 3).V_t=0.1V and I_t=O.2 nA.*

An important aspect of the surface oxide is that, contrary to the CO-covered surface; the oxygen-induced structures hardly evolve in time. In oxygen atmosphere the surface is much less mobile than in a CO-rich flow, as illustrated by the images in figure 6.10. Between the recording of the first and the last image in the series a time interval of 2 h passed. The crosses in the images indicate the same location on the surface.

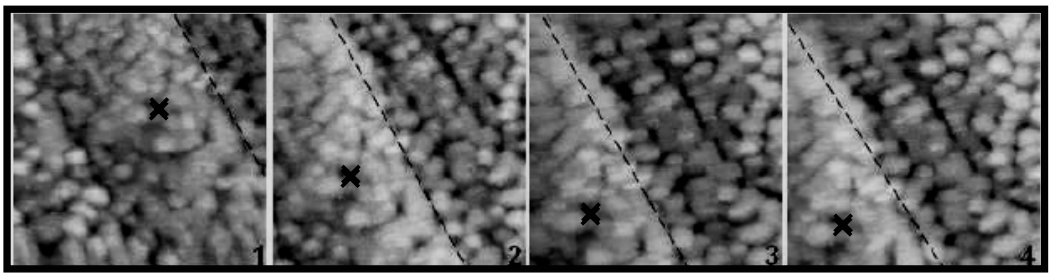

Figure 6.10: *STM images (100 nm × 100 nm) showing the absence of evolution in time of the Pt(100) surface in an O_2-flow of P = 1.25 bar at T =408 K.*

6.3.3 Pt(100) in a CO+O_2 mixture, during CO oxidation

Langmuir-Hinshelwood versus Mars-van-Krevelen reaction kinetics

Although the reversible oxidation and reduction of the Pt(100) surface in O_2 and CO atmospheres is strongly reminiscent of the behaviour of Pt(110) and Pt(111), there are also important differences between these low-index platinum surfaces. The most important difference is that only in a few experiments (3 out of 30) on Pt(100) we have measured a small, stepwise increase in CO_2 production rate and a simultaneous, modest step down in CO partial pressure at a sufficiently high partial pressure of O_2 and a sufficiently low pressure of CO. The kinetics of such an experiment, performed at P_{total} = 1.25 bar and T = 418 K is depicted in figure 6.11. First, the sample has been in a CO-rich flow. At t = 769 s we have switched to an O_2-rich flow. The CO_2 production rate followed the increasing trend of the oxygen partial pressure. The reaction rate passed through a maximum value at t = 769 s, after which it followed the decreasing trend of the CO partial pressure. As we have seen several times before in this thesis, this sequence is characteristic for the Langmuir-Hinshelwood reaction mechanism, for which the reaction rate is at its maximum when we have equal coverages of CO and O. At t = 3938 s (indicated by the arrow) we observe a sudden step up in the CO_2 production. The upward step in the reaction rate is accompanied by a small, downward step in the CO partial pressure, as can be seen in the enlarged graph in figure 6.11 (b). For the other platinum and palladium surfaces such steps in reactivity have been found to be associated with the formation of a new structure, namely a surface oxide. On these

surface oxides the oxidation reaction was found to follow the Mars van Krevelen mechanism: each CO molecule reacts with an oxygen atom from the surface oxide lattice.

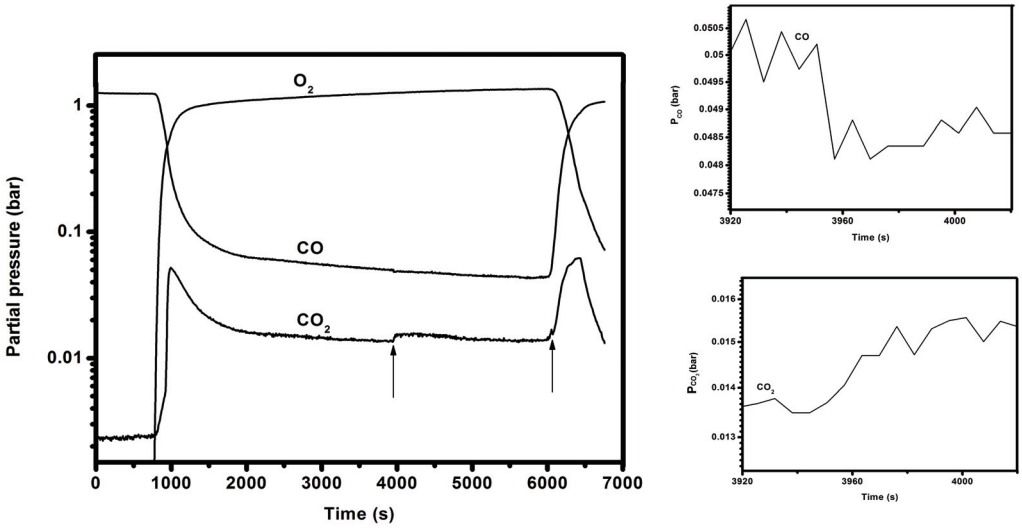

Figure 6.11: *CO oxidation reaction kinetics on Pt(100) at a total pressure of 1.25 bar and T= 418 K. The sequence shows Langmuir-Hinshelwood behaviour for times up to t = 3938 s and for times after t = 6091 s and Mars-van-Krevelen behaviour for intermediate times. The MvK behaviour is associated with the formation of a surface oxide.*

Figure 6.12 shows an attempt to fit the measured production rates of CO_2 with a simple model, based solely on Langmuir-Hinshelwood kinetics. The left panel shows a time sequence of the CO_2 partial pressures P_{CO_2} similar to that in Fig. 6.11, this time displayed on a linear pressure scale. The right panel represents the best fit to this data according to the LH mechanism, modeled by the following equations for the reaction rate *R*.

$$R = P_1 \frac{\sqrt{p_{O_2}}\, p_{CO}}{\left(P_2\sqrt{p_{O_2}} + p_{CO}\right)^2} \ , \tag{5.1}$$

in which we have defined

$$P_1 = \frac{k_3\sqrt{K_{O_2}}}{K_{CO}} \text{ and } P_2 = \frac{\sqrt{K_{O_2}}}{K_{CO}} \ . \tag{5.2}$$

In this calculation the partial pressures p_{O_2} and p_{CO} have been taken from the experiment and the constants k_3 and P_2 have been used as fitting parameters. Although the fit to the two LH peaks is not perfect, it is clear

that the model catches the essence of the LH behaviour. Obviously, the stepwise increase and decrease of the reaction rate at 9600 s and 10800 s respectively, which reflect the transition between LH-kinetics and MvK-kinetics associated with the oxidation of the surface, are not described by this LH-model.

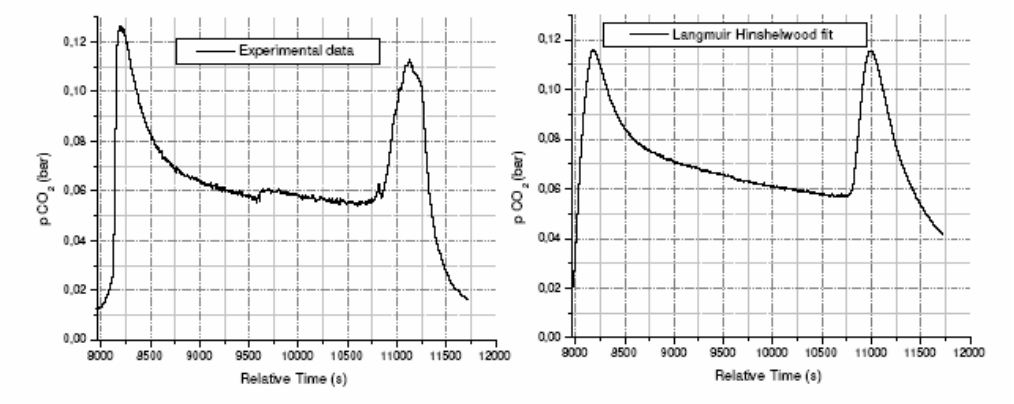

Figure 6.12: *Measured CO oxidation rate on Pt(100), as recorded by the mass 44 CO_2 signal from the mass spectrometer at P_{total} = 1.25 bar and 423 K (left panel) and the calculated reaction rate according to Langmuir-Hinshelwood kinetics (right panel).*

As mentioned already, the upward step in the reactivity, which is associated with the formation of the oxide, has been observed only in three experiments, in which we performed repeated cycles of exposure to CO and O_2. Interestingly, these three experiments were the *very first* experiments performed on a new, freshly polished and UHV-prepared Pt(100) sample. After these initial three experiments we have never been able to again provoke the increase in CO_2 production, even though we have fully reproduced the reaction conditions and the sample cleaning procedures of the initial experiments. This observation presents a strong indication that in this case the history of the surface plays a key role in the catalytic activity. In particular, the initial step density of the freshly prepared Pt(100) surface (Fig. 6.3) was lower than the step density after one or more cycles of oxidation and reduction of the Pt surface. We speculate that the Pt(100) surface exhibits a relation between step density and oxidation conditions, similar to what we have found on Pd(100) (Chapter 3), in the present case rapidly shifting the critical CO pressure for oxidation of the Pt surface at the temperatures and oxygen pressures used in our experiment to lower values. As we have seen before for other surfaces and as we will see for Pt(100), the step in reactivity, i.e. the difference in the production rate of CO_2 between the MvK and LH mechanisms, is smaller at lower CO pressures. In the present case the step in P_{CO_2} has been going down from a small value to basically zero, meaning that we can no longer use the measured reactivities

to be sure whether the catalytic system is operating on the LH branch or on the MvK branch.

Langmuir-Hinshelwood kinetics

Figure 6.13 depicts the partial pressure of the reactant gases CO and O_2, and the reaction product CO_2, as were measured by the mass spectrometer in an experiment that started at t = 0 s in a CO-rich flow at a total pressure of 1.25 bar and 368 K. At t = 3716 s the O_2 pressure was raised and the CO_2 signal initially increased accordingly, then reached a maximum value at t = 4229 s (indicated by arrow 1), after which it decreased, following the reduction in the CO pressure as we switched to an O_2 rich flow. Similar to the other platinum group metals, CO oxidation on Pt(100) follows the Langmuir-Hinshelwood mechanism over a certain regime of partial pressures. According to this mechanism the maximum value in CO_2 production corresponds to equal coverages of reactant gases $\theta_{CO} = \theta_O = 0.5$. At t = 7931 s we increased the CO pressure again. Consequently the CO_2 pressure also increased and again reached a maximum at t=8559s (arrow number 2), where we again assume to have equal coverages, $\theta_{CO} = \theta_O = 0.5$. At high CO pressures the CO_2 signal decreased in time due to the poisoning of the surface by the high coverage of CO.

Arrow 3 indicates a modest increase in CO_2 pressure that occurred when we increased the O_2 partial pressure at t = 15333 s to 0.22 bar. Since the total pressure is constant the CO partial pressure decreased hand in hand with the increase in O_2 pressure, the CO:O_2 partial pressure ratio becoming 3.5. Interestingly, 2107 s later, at t = 17440 s, we observed a spontaneous, big step in the reaction rate (arrow 4). Coinciding with the increase in CO_2 pressure we noticed modest reductions in the CO and O_2 partial pressures. After this big increase the reaction rate was steady as long as we kept the partial pressures of CO and O_2 unchanged. At t = 19604 s (arrow 5) we further increased the O_2 partial pressure. This resulted in a strong decrease in the reaction rate, similar to what we always measure at high oxygen pressures (e.g. the reduction after the LH-peak at arrow 1).

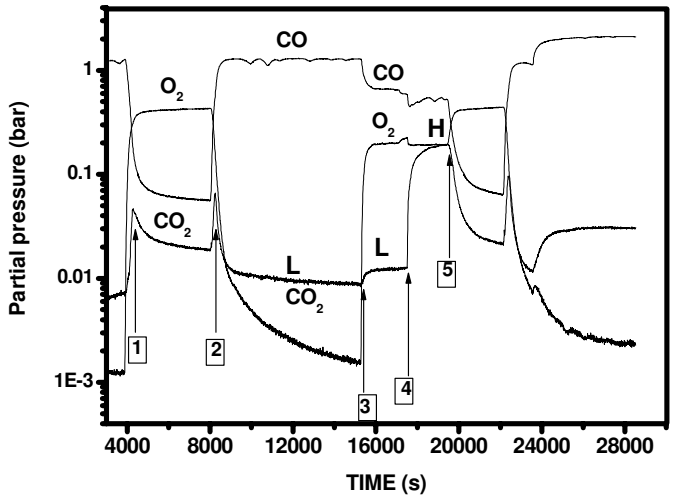

Figure 6.13: *Reaction kinetics for CO oxidation at a total pressure of 1.25 bar and 368 K. The letters L indicate the regime where the reaction rate is low and the letter H corresponds to the maximum in the reaction rate.*

The increase in the reaction rate at arrow 4 is quite spectacular. In the particular example of Fig. 6.13, a minor variation took place in the CO/O_2 partial pressure ratio in the 500 s prior to the sudden increase in reactivity. We have reproduced the stepwise increase in reactivity several times and have verified that the pressure variation of Fig. 6.13 does not form a necessary ingredient of this behaviour. In view of the previous results obtained with our high-pressure STM and SXRD experiments on CO oxidation catalysis, one would expect that the dramatic increase in reactivity would be accompanied by a sudden change in the surface structure. Figure 6.14 repeats a part of the time trace of the partial pressure of CO_2 from Fig. 6.13 and combines it with the structure of the surface as observed simultaneously with the STM. Apart from modest fluctuations of the island shapes, the images obtained prior to and after the change in reactivity are close to identical (images S, S_1, S_2); they all show the unreconstructed Pt(100)-(1x1) surface with adatom islands. Only when we exposed the surface to high oxygen pressures, towards the end of the time interval of Fig. 6.14, did the STM image change and show a pattern typical for a surface oxide (image S_3), but this was under conditions at which the reaction rate was low again.

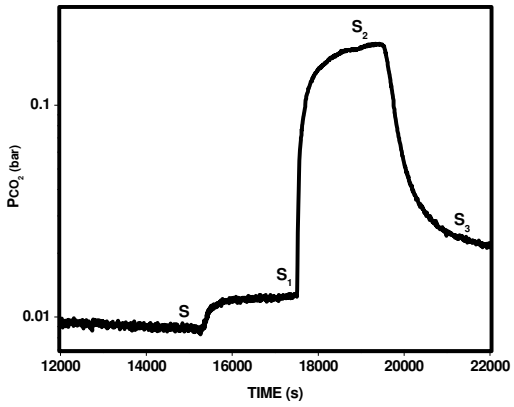

(a)

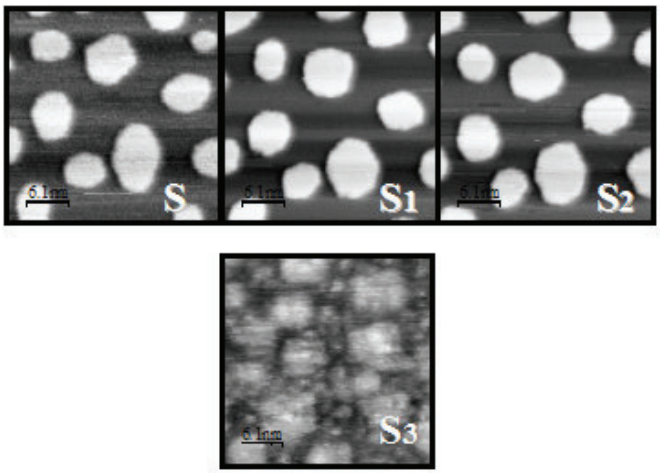

(b)

Figure 6.14: *Time sequence of the CO_2 production rate around the sudden increase in rate, taken from Fig. 6.13, combined with simultaneously recorded STM images (30.5 nm × 30.5 nm). Image S has been acquired in the initial, CO-rich flow. Image S_1 shows the surface in a 3.5:1 CO/O_2 mixture. Image S_2 corresponds to the highest observed reactivity. Images S, S_1 and S_2 are very similar. They all show the metallic surface with adatom islands. Finally, image S_3 shows a rougher surface, characteristic for the presence of a disordered surface oxide. V_t=0.9V and I_t=0.2 nA.*

Steps are often considered as the special reaction sites in heterogeneous catalysis. One might wonder whether changes in step density could be responsible for the sudden increase in reaction rate. However, as the selected images in Fig. 6.14 already indicated, the variation in step density over the time interval in which the strong increase takes place in reactivity was as good as zero. This visual impression is confirmed by a quantitative analysis of the step density as counted in the STM images, which is shown in

Fig. 6.15, together with the CO_2 partial pressures. It is only near the end of the sequence, after the maximum in reactivity, under a high partial pressure of oxygen at which the STM images (c.f. image S_3 in Fig. 6.14) show that the surface oxidized, that the roughness suddenly increased.

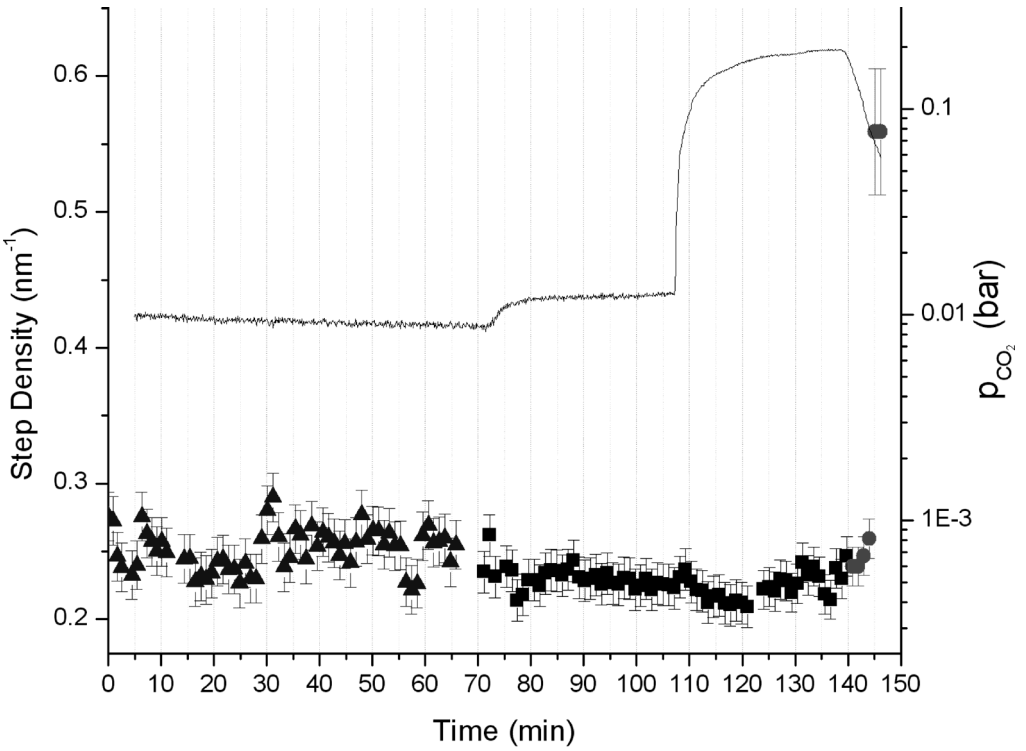

Figure 6.15: *Measured time dependence of the step density, illustrating the absence of a variation in this quantity while the CO_2 partial pressure goes through the stages shown before, including the sudden, strong increase in reactivity.*

We have repeated this experiment of stepping up from a CO-rich flow to the same O_2:CO pressure ratio of 0.7 ± 0.3 at a few different temperatures. In each case, we observed a high reactivity and except for the highest temperature, the high reactivity was reached by a spontaneous, upward step (factor 14 to 19) after a significant delay time. The temperature dependence of this delay time is shown in table 6.1. The temperature dependence of the delay can be interpreted as the signature of a thermally activated process (Arrhenius behaviour) with an activation energy of 1.2 ± 0.3 eV.

Starting from the maximum in the reactivity and slowly increasing the partial pressure of oxygen we noticed the frequent appearance and disappearances of small, adatom-island-like structures, as is illustrated in figure 6.17.As seen from Figure 6.18 these structures have heights in the order of 2.8 ± 0.2Å, which does not correspond to the step height of Pt(100).

Temperature (K)	Delay (s)	P_{CO_2} (low reactivity) (bar)	P_{CO_2} (high reactivity) (bar)
365	1052	0.025	0.445
368	2209	0.019	0.363
398	130	0.011	0.213
408	117	0.035	0.504
423	4		0.547

Table 6.1: *Temperature dependence of the delay time between setting an O_2:CO partial pressure ratio of 0.7 ± 0.3 and observing a spontaneous upward step in reactivity.*

Image 1 has been acquired before the partial pressure of oxygen was increased. The two circles indicate regions where new structures, labelled I, II and III, will show up simultaneously with the increase in O_2 flow in images 2 and 3. First the structure I has appeared in image 2. In image 3, which has been recorded immediately after image 2, structure I has disappeared again, but the other two structures labelled II and III have been formed. In the next image (4) also structures II and III have disappeared. All these images have been acquired directly after each other. The time necessary to record an image was about 40 s. This implies that in the high reactivity state the surface was extremely mobile, new structures showing up and disappearing within the time of a single image. Actually these processes took place so fast that was difficult to follow them with our STM. Since the extra structures described here were not present before the increase in the O_2 partial pressure we conclude that their formation is due to the oxygen. Since as discussed before these structure appears only when we increase the O_2 pressure and have a step height higher than the step height of Pt(100) we may speculate that they are oxidic species.

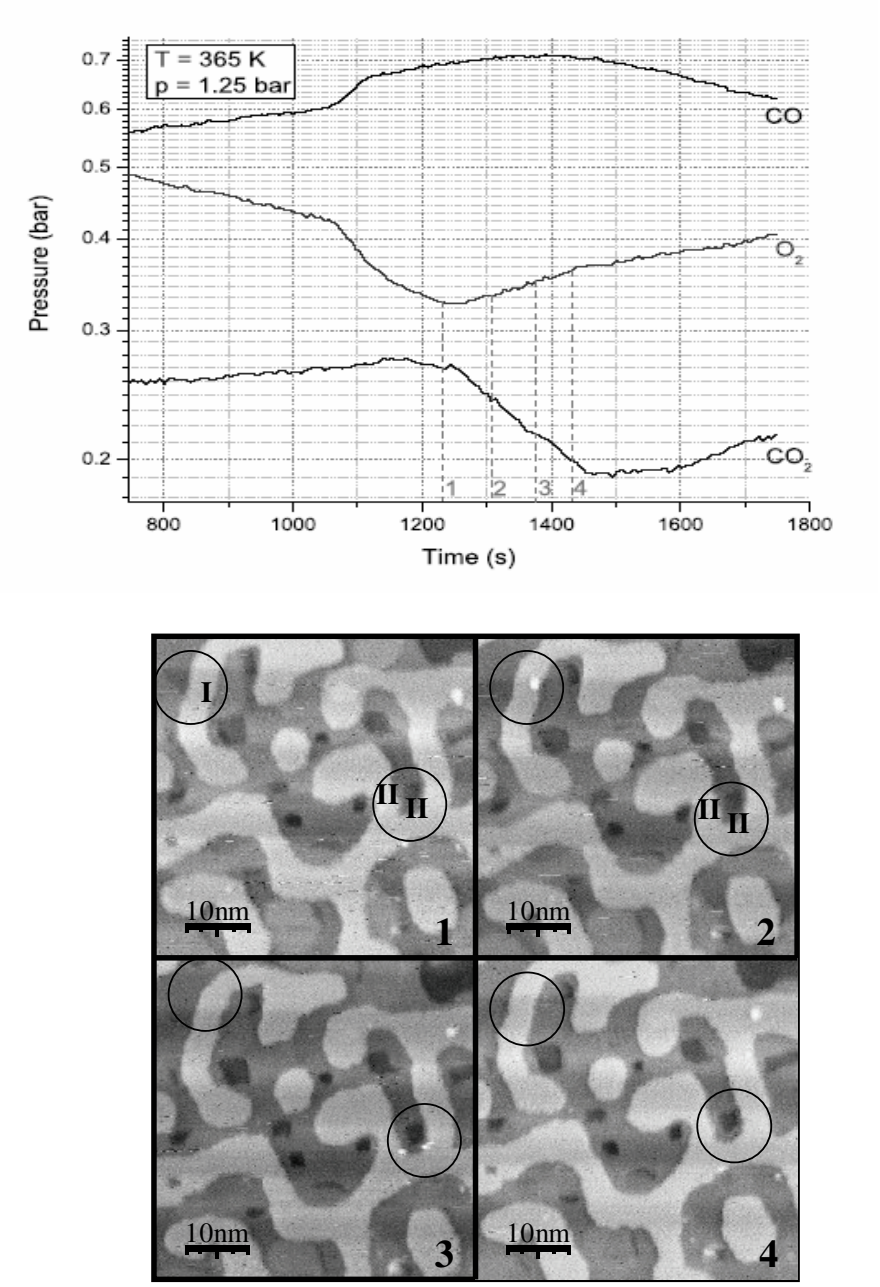

Figure 6.17: *STM images (50nm×50nm) recorded while the reaction rate was near its maximum and the oxygen partial pressure was increased. The circled regions illustrate the frequent formation and removal of adatom-island-like structures. The numbers in the top panel indicate the times and partial pressures of O_2, CO and CO_2 when the images were recorded, T=373 K. V_t=0.9V and I_t=0.2 nA.*

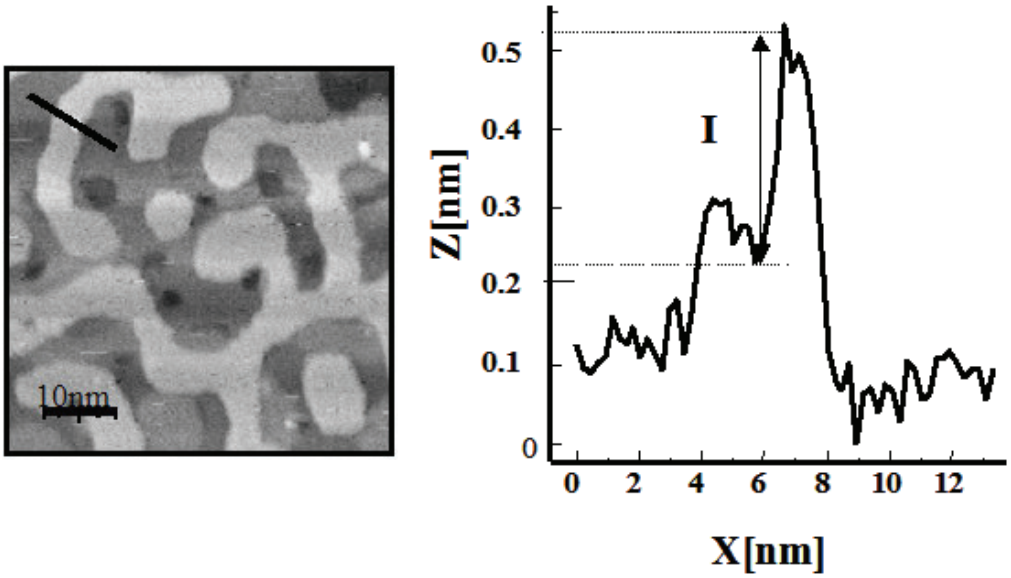

Figure 6.18: *Profile along the line in image 2. The height of the structure I does not correspond to the step height of Pt(100).*

6.3.4 Bistability and hysteresis

We have shown in previous chapters of this thesis for other model catalyst surfaces that if we plot the reaction rate (CO_2 pressure) as a function of CO pressure all experimental data for a particular surface fall on two branches: a low-reactivity branch, which is associated with a metallic surface and a high-reactivity branch, corresponding to some form of surface oxide. This behaviour has been observed for all three palladium surfaces investigated in Chapter 2 and for the Pt(111) surface, studied in Chapter 5, as well as for Pt(110) [21]. The case for Pt(100) is different in two respects. First, the range of CO pressures over which the surface oxide is more stable than the metal (at the relatively low temperatures of our experiment) is much smaller on Pt(100) than on the other platinum and palladium surfaces. In Fig. 6.19 we show three plots of CO_2 pressure versus CO pressure on Pt(100). Whereas in panels (a) and (b) a short oxide branch can be seen at low CO pressures, such a branch is no longer visible in panel (c). In fact, the only measurements in which the oxide branch was observed corresponded to the very first three oxidation-reduction cycles of the surface, after it had been prepared in our UHV system for the first time. As we already argued in Sect. 6.3.3, the maximum CO pressure at which the oxide was stable was probably reducing after repeated oxidation-reduction cycles, because of the influence of the steadily increasing density of steps. Interestingly, the STM images, discussed in Sect. 6.3.3, showed that at the lower CO partial pressures that we could reach in our experiment the surface still oxidized.

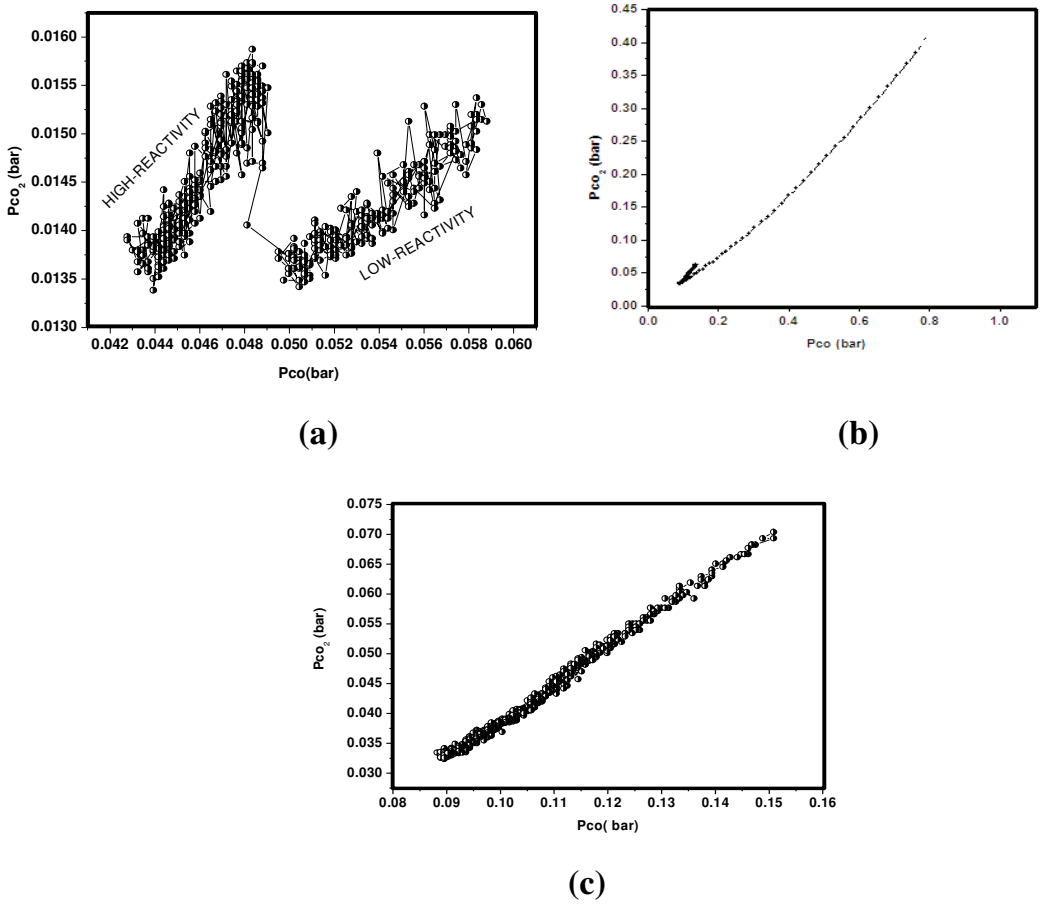

Figure 6.19: *CO_2 partial pressure (reaction rate) plotted as a function of CO pressure from three different sets of measurements on Pt(100). The reaction conditions were (a) P_{total} = 1.25 bar, T = 423K; (b) P_{total} = 1.75 bar, T = 430 K (c) and P_{total} = 1.25 bar, T = 423 K. Graphs a and b illustrate the extremely limited range of CO partial pressures over which the oxide branch could be observed on Pt(100); in graph c no oxide branch can be distinguished anymore.*

However, as we can see from the 'oxide' branch in panels (a) and (b) of Fig.6.19, at these low CO pressures the Mars-van-Krevelen mechanism, responsible for the oxide branch, was so close to its intersection with the Langmuir-Hinshelwood branch, that no upward (downward) step could be measured in the CO_2 signal when the surface oxidized (reduced).

The second difference between the kinetics on Pt(100) and that on the other surfaces investigated in this thesis is that, as discussed in the previous section, there is a second rapid increase/decrease in reactivity, which occurred at much higher CO pressures. When again plotted in the form of P_{CO_2} versus P_{CO}, also this part of the behaviour indicates clear bistability (Fig.6.20).

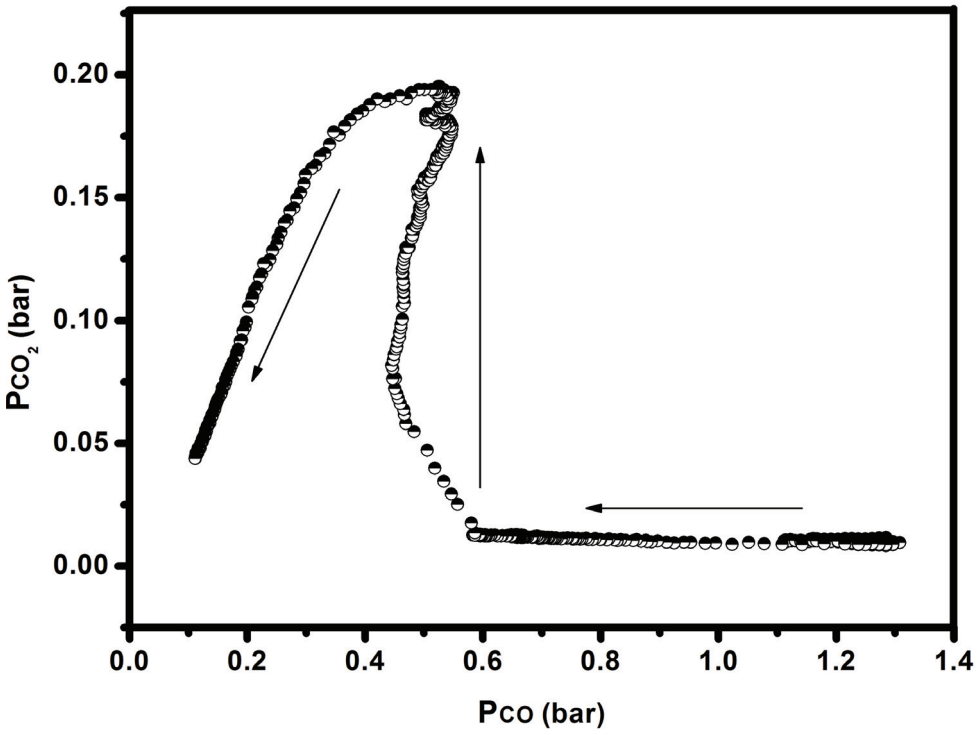

Figure 6.20: *CO_2 partial pressure (reaction rate) plotted as a function of CO pressure in the high P_{CO}-regime on Pt(100) at P_{total} = 1.25 bar and T = 368 K, illustrating the Langmuir-Hinshelwood bistability of this surface at atmospheric pressures.*

However, in this case, we have observed no changes in the STM images, indicating that this step was *not* induced by a phase transition of the metal substrate. In fact, this high-P_{CO} instability took place completely on the Langmuir-Hinshelwood branch. From this we infer that the observed transition is that from a mixed, two-dimensional overlayer of chemisorbed CO-molecules and O-atoms with a high CO-coverage to one with a low O-coverage. In other words, this instability is identified as the 'classic' fingerprint of the Langmuir-Hinshelwood bistability [23]. Several interesting questions remain. The complete absence of changes in the STM images indicates that we have been insensitive to the change in overlayer composition. Possibly, this means that the overlayer has been mixed on an atomic/molecular scale or, in case of segregated overlayer islands of adsorbed CO and adsorbed O, the dynamics of these islands has been so much faster than the imaging rate of the STM that the images have completely averaged over the islands. High-speed imaging or other forms of high-speed STM data acquisition may be used to push the time resolution on this by five or more orders of magnitude. However, at the high conversion

rates obtained in the present experiment, this may still not be enough to resolve the dynamics and/or structure of the adsorbate overlayer.

6.4 Conclusions

The study of CO oxidation by O_2 on Pt(100) at atmospheric pressures and elevated temperature has proved to be an interesting subject. Under these reaction conditions the Pt(100) surface behaves different compared to the other low-index surfaces of platinum, Pt(111) and Pt(110). We have observed that the hex-reconstruction of Pt(100) is lifted by exposure to CO, O_2 or mixtures of these gasses. Although the STM images clearly have indicated that at high O_2 pressures and low CO pressures, the surface is oxidized, the reaction kinetics have indicated that the corresponding Mars-van-Krevelen branch at low CO pressures is so close to the reactivity on the Langmuir-Hinshelwood reaction branch of the reduced surface that the two mechanisms could be distinguished from each other on the basis of the reaction kinetics measurements only in the first few oxidation-reduction cycles starting from a freshly polished surface. In later cycles the surface switched back to the LH branch at too low a CO pressure to observe a step in the reactivity. In addition to this combination of stepwise changes in STM images without changes in the reaction rate we have also observed stepwise changes in reaction rate accompanied by a complete absence of changes in the STM images. This new combination has been observed at higher CO pressures and we ascribe it to the traditional bistability on the LH branch. Although the rate constant for the CO_2 production is higher for the oxide than for the metal, the reaction can run at much higher CO pressures on the metal than on the oxide, so that the maximum production rate on the metal is much higher than the maximum rate on the oxide.

6.5 References

[1] X.C.Guo, A.Hopkinson, J.M.Bradley and D.A.King, *Surf.Sci.***278** (1992) 263.
[2] S.Hangstrom, H.B.Lyon and G.A.Somorjai, *Phys.Rev.Lett.***15** (1965) 171.
[3] D.G.Fedak and N.A.Gjostein, *Phys.Rev.Lett.***16** (1966) 171.
[4] D.G.Fedak and N.A.Gjostein, *Surf. Sci*. **8** (1967) 77.
[5] J.T.Grant, *Surf.Sci.***18** (1969) 228.
[6] C.Berg, H.J.Venvik, F.Strisland, A.Ramstad, A.Borg, *Surf.Sci.***409** (1998) 1.
[7] R.J.Behm, P.A.Thiel, P.R.Norton, G.Ertl, *J.Chem.Phys.***78** (1983) 7437.
[8] P.A.Thiel, R.J.Behm, P.R.Norton, G.Ertl, *J.Chem.Phys.***78** (1983) 7448.
[9] K.Griffiths, T.E.Jackmann, J.A.Davies, P.R.Norton, *Surf.Sci.138* (1984) 113.
[10] P.R.Norton, K.Griffiths, P.E.Binder, *Surf.Sci*.**138** (1984) 125.
[11] W.Hosler, R.J.Behm, E.Ritter, *J.Rev.Dev*.**30** (1986) 403.
[12] E.Ritter, R.J.Behm, G.Potschke, J.Wintterlin, *Surf.Sci*.**181** (1987) 403.
[13] P.Gardner, M.Thushaus, R.Martin, A.M.Bradshaw, *Surf.Sci*.**278** (1990) 112.
[14] K.Mase, Y.Murata, *Surf.Sci.***277** (1992) 97.
[15] A.Borg, A.M. Hilmen, E.Bergene, *Surf.Sci*.**306** (1994) 10.
[16] C.Berg, H.V.Venvik, F.Strisland, A.Ramstad, A.Borg, *Surf.Sci.***409** (1998) .
[17] A.Sinsarp, Y. Yamada, M. Sasaki, S. Yamamoto, *Appl.Surf.Sci.***237** (2004) 587.
[18] V.Fiorentini, M.Methfessel and M.Scheffler, *Phys.Rev.Lett*.**71** (1993) 1051.
[19] R.H.M. Smit, C. Untiedt, A.I. Yanson and J.M. van Ruitenbeek, *Phys. Rev. Lett.* **87** (2001) 266102.
[20] P.A.Thiel, R.J.Behm, P.R.Norton, and G.Ertl, *Surf.Sci.***121** (1982) L553.
[21] B. L. M. Hendriksen , PhD Thesis,Leiden University 2003.
[22] H.Hopster, H.Ibach and G.Comsa, *J.Catal.* **46**(1977) 37.
[23] H. Conrad, G. Ertl and J. Küppers, *Surf.Sci.***76** (1978) 323.